

# Water Adsorption at the Tetrahedral Titania Surface Layer of SrTiO<sub>3</sub>(110)-(4 × 1)

Zhiming Wang,<sup>†</sup> Xianfeng Hao,<sup>†</sup> Stefan Gerhold,<sup>†</sup> Zbynek Novotny,<sup>†</sup> Cesare Franchini,<sup>‡</sup> Eamon McDermott,<sup>§</sup> Karina Schulte,<sup>†</sup> Michael Schmid,<sup>†</sup> and Ulrike Diebold\*,<sup>†,†</sup>

<sup>†</sup>Institute of Applied Physics, Vienna University of Technology, 1040 Vienna, Austria

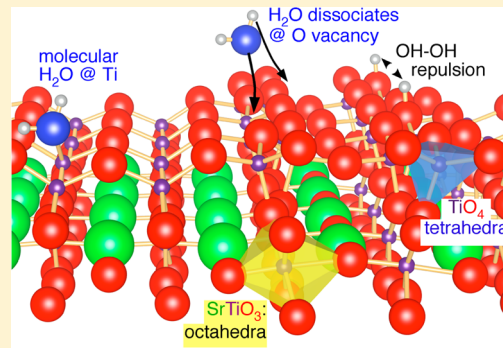
<sup>‡</sup>Faculty of Physics & Center for Computational Materials Science, University of Vienna, 1090 Vienna, Austria

<sup>§</sup>Institute of Materials Chemistry, Vienna University of Technology, 1060 Vienna, Austria

<sup>†</sup>MAX IV Laboratory, Lund University, SE-221 00 Lund, Sweden

## Supporting Information

**ABSTRACT:** The interaction of water with oxide surfaces is of great interest for both fundamental science and applications. We present a combined theoretical (density functional theory (DFT)) and experimental (scanning tunneling microscopy (STM) and photoemission spectroscopy (PES)) study of water interaction with the two-dimensional titania overlayer that terminates the SrTiO<sub>3</sub>(110)-(4 × 1) surface and consists of TiO<sub>4</sub> tetrahedra. STM and core-level and valence band PES show that H<sub>2</sub>O neither adsorbs nor dissociates on the stoichiometric surface at room temperature, whereas it does dissociate at oxygen vacancies. This is in agreement with DFT calculations, which show that the energy barriers for water dissociation on the stoichiometric and reduced surfaces are 1.7 and 0.9 eV, respectively. We propose that water weakly adsorbs on two-dimensional, tetrahedrally coordinated overlayers.



## 1. INTRODUCTION

The discovery of photochemical water splitting on SrTiO<sub>3</sub> with no external bias under UV irradiation has motivated much research into the interaction of water with this material.<sup>1,2</sup> More recent reports of overall water splitting on SrTiO<sub>3</sub> with a NiO cocatalyst has renewed this interest.<sup>3,4</sup> A fundamental question is simply whether water adsorption is molecular or dissociative.<sup>5–13</sup> For SrTiO<sub>3</sub>(100), photoemission spectroscopy (PES), high-resolution electron energy loss spectroscopy (HREELS), and temperature-programmed desorption (TPD) studies show that water does not adsorb on the stoichiometric surface at room temperature (RT) although molecular water adsorption has been observed below 150 K. However, dissociative adsorption was observed for water on both Ar<sup>+</sup>-bombarded and vacuum-fractured SrTiO<sub>3</sub>(100) surfaces.<sup>10–12</sup> Theoretical calculations are in agreement with experimental results predicting molecular water adsorption on the stoichiometric SrTiO<sub>3</sub>(100) surface.<sup>14–16</sup>

In this context it is important to note that SrTiO<sub>3</sub>(100) forms a wide variety of reconstructions, which depend strongly on the preparation conditions and sample history. Various groups report different results;<sup>17</sup> thus, it is not always straightforward to connect water adsorption experiments to the actual surface structure. Recently, the SrTiO<sub>3</sub>(110) surface has received significant attention.<sup>18–22</sup> It was found that the SrTiO<sub>3</sub>(110) surface can be prepared reproducibly and reversibly with a variety of surface structures.<sup>18,20</sup> The ( $n \times$

1) ( $n = 3–6$ ) series of reconstructions was solved by transmission electron diffraction and direct methods and confirmed and refined by density functional theory (DFT) calculations and scanning tunneling microscopy (STM).<sup>19,21</sup> Thus, a reliable structural model is available for this surface.

The SrTiO<sub>3</sub>(110) surface is polar, as a SrTiO<sub>3</sub> crystal can be considered as a stack of equidistant (SrTiO)<sup>4+</sup> and (O<sub>2</sub>)<sup>4-</sup> planes along the [110] direction.<sup>23</sup> Generally, polar surfaces are considered more reactive than nonpolar surfaces.<sup>24,25</sup> In this case, however, the polarity is compensated via the formation of a (4 × 1) reconstruction with a nominal stoichiometry of (Ti<sub>1.5</sub>O<sub>4</sub>)<sup>2-</sup>. The reconstruction consists of 6- and 10-membered rings of corner-shared TiO<sub>4</sub> tetrahedra residing directly on the bulk-like SrTiO<sub>3</sub>, which consists of octahedrally coordinated Ti (Figure 1a). The surface reconstruction can be tuned by varying the surface stoichiometry,<sup>20,26</sup> forming a homologous series of ( $n \times 1$ ) ( $n = 3–6$ ) with a variable number of tetrahedra per ring.<sup>19,21</sup> Recently, we reported that quasi-long-range ordered antiphase domains are formed on the (4 × 1) surface.<sup>27</sup> The domain boundaries are decorated by defect pairs consisting of a Ti<sub>2</sub>O<sub>3</sub> vacancy cluster and a Sr adatom; the presence of these pairs preserves the polarity compensation.

**Received:** August 7, 2013

**Revised:** November 22, 2013

**Published:** November 25, 2013



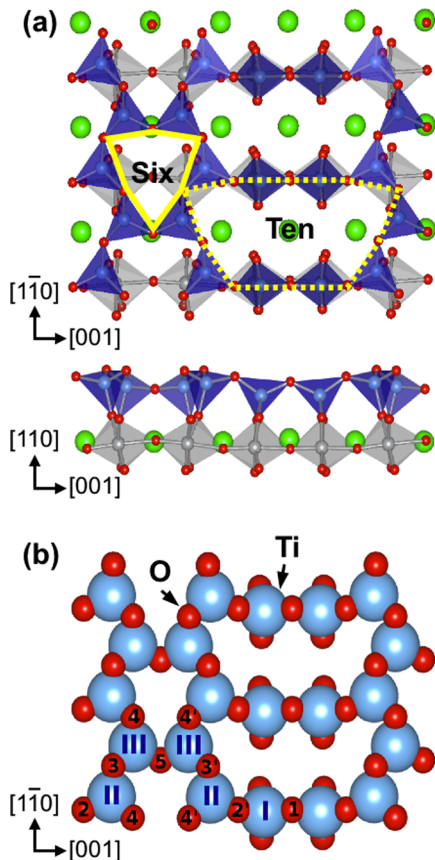


**Figure 1.** Model of the SrTiO<sub>3</sub>(110)-(4×1) surface. (a) Top and side views. The reconstructed layer consists of a network of darker TiO<sub>4</sub> tetrahedra (blue) forming 6- and 10-membered rings on top of the SrTiO<sub>3</sub>(110) substrate, which contains TiO<sub>6</sub> octahedra (lighter, gray). Large, medium, and small spheres denote Sr, Ti, and O atoms, respectively. (b) Top view of the topmost reconstructed layer with the surface Ti and O atoms labels used in the present study.

In recent reports, periodically arranged, tetrahedrally coordinated MeO<sub>4</sub> (Me = Ti, Si) units have emerged as a common feature on several oxide surfaces.<sup>19,21,28–31</sup> For example, such units form one-dimensional rows at the anatase TiO<sub>2</sub>(001)-(1×4) and rutile TiO<sub>2</sub>(110)-(1×2)-Ti<sub>2</sub>O<sub>3</sub> surfaces.<sup>28,29</sup> For anatase (001), a high reactivity toward water adsorption was reported;<sup>32,33</sup> this surface was also identified as the most active one in photocatalytic reactions,<sup>34</sup> although it remains controversial whether the reconstructed or the unreconstructed anatase (001) surface is the most active phase.<sup>35</sup> Well-ordered, ultrathin silica structures consisting of SiO<sub>4</sub> units have also been reported<sup>36</sup> that bear resemblance to the two-dimensional network on the SrTiO<sub>3</sub>(110)-(n×1) ( $n = 3–6$ ) and rutile TiO<sub>2</sub>(100)-c(2×2) surfaces.<sup>19,21,31</sup> It should be noted, however, that Ti in bulk TiO<sub>2</sub> and SrTiO<sub>3</sub> is octrahedrally coordinated, in contrast to SiO<sub>2</sub>, which forms tetrahedra also in the bulk.

In this article we present a combined experimental (STM and PES) and theoretical (DFT) investigation of water adsorption on stoichiometric and reduced SrTiO<sub>3</sub>(110) surfaces with a two-dimensional tetrahedrally coordinated (4×1) reconstructed layer. Both experimental and theoretical results clearly show that water dissociates on the surface with oxygen vacancies (V<sub>O</sub>'s), while water neither adsorbs nor dissociates on the stoichiometric surface at room temperature

(RT). Generalizing our result, we propose that two-dimensional, tetrahedrally coordinated overlayers on oxide materials interact only weakly with water.

## 2. MATERIALS AND METHODS

**2.1. Experimental Details.** STM measurements were performed in two ultrahigh vacuum (UHV) chambers equipped with a SPECS Aarhus STM at RT and an Omicron low-temperature (LT) STM at 78 K, respectively (see refs 37 and 38 for more details). Synchrotron radiation photoemission spectroscopy experiments were performed at beamline I311 at the MAX IV Laboratory.<sup>39</sup> The pressure in all UHV systems was better than  $1 \times 10^{-10}$  mbar. Nb-doped (0.5 wt %) SrTiO<sub>3</sub>(110) single crystals were purchased from MaTeck, Germany. The clean surface was prepared by cycles of Ar<sup>+</sup> sputtering (1 keV, 5 μA, 10 min) followed by annealing in  $2 \times 10^{-6}$  mbar oxygen at 900 °C for 1 h.<sup>40</sup> The samples were heated by electron bombardment (13 mA, 900 V) or by passing alternating current through the crystal, and the temperature was monitored with an infrared pyrometer. The surface reconstruction was checked by low-energy electron diffraction (LEED) and was adjusted by depositing Sr or Ti on the surface at RT followed by annealing until a sharp (4×1) LEED pattern was observed.<sup>20</sup> The surface was exposed to atomic H by backfilling the chamber with H<sub>2</sub> while keeping a hot tungsten filament in line of sight with the sample. The hydrogen cracking efficiency in our setup is estimated to be 5% with the W filament temperature about 2000 °C.<sup>41</sup> The density of H atoms is around 0.1 per nm<sup>2</sup> after dosing at a H<sub>2</sub> partial pressure of  $1 \times 10^{-6}$  mbar for 5 min with the sample at room temperature. Deionized H<sub>2</sub>O was cleaned by repeated freeze-pump-thaw cycles and dosed by backfilling the UHV chamber through a leak valve. The purity of the water vapor was checked by mass spectrometry. All photoemission spectra in this paper were collected with emission normal to the sample plane; the angle between the sample normal and the incoming X-rays was 54.7°. Photon energies were 605 and 45 eV for core-level and valence band photoemission spectroscopy, respectively. The binding energies were calibrated with respect to the Fermi level of a clean Mo sample plate, on which our sample was mounted.

**2.2. Computational Details.** The first-principles calculations were performed using the projector augmented-wave method as implemented in the Vienna ab initio simulation package (VASP) code,<sup>42,43</sup> using the Perdew–Burke–Ernzerhof (PBE)<sup>44</sup> approximation to treat the exchange-correlation functional within the DFT. The kinetic energy cutoff for the plane waves expansion was set to 600 eV, and reduced to 400 eV for the nudged elastic band (NEB) calculations as detailed below. To improve the description of dispersion forces, which are expected to play an important role in H<sub>2</sub>O physisorption phenomena and are not correctly accounted for in standard DFT, we have employed two alternative corrections: (i) the DFT-D2 method of Grimme<sup>45–47</sup> and (ii) the modified version of van der Waals DFT (vdW-DFT), adopting the recently introduced functional optB86b-vdW.<sup>48</sup>

Our surface calculations are based on the SrTiO<sub>3</sub>(110)-(4×1) structural model proposed by Enterkin et al.<sup>19</sup> To weaken the interaction between the water and its periodic image we have adopted a large (4×2) supercell (Figure 1), which is constructed by doubling the (4×1) model along the [110] direction. We have used a symmetric slab consisting of 13 layers separated by a vacuum layer of 12 Å (total thickness 32 Å). A pair of H<sub>2</sub>O molecules was symmetrically adsorbed on both

sides of the slab. During structural optimization all atoms were allowed to relax until all components of their residual forces were less than  $0.02 \text{ eV} \text{\AA}^{-1}$ , except for the atoms in the central three layers, which were kept fixed in their bulk positions. We have used the fully optimized PBE lattice constant  $3.945 \text{ \AA}$  (very close to the corresponding experimental one,  $3.905 \text{ \AA}$ ) and a  $(2 \times 3 \times 1)$  Monkhorst–Pack k-point mesh (reduced to  $1 \times 1 \times 1$  for the NEB runs) for the Brillouin zone integrations.

The oxygen vacancy formation energy  $E_f(V_O)$  is computed as  $E_f(V_O) = 1/2[E_{\text{TOT}}(2V_O) - E_{\text{TOT}} + E(O_2)]$  where  $E_{\text{TOT}}$  refers to the DFT total energy of the clean symmetric slab,  $E_{\text{TOT}}(2V_O)$  denotes the DFT total energy of the symmetric slab containing two  $V_O$ 's, and  $E(O_2)$  indicates the DFT energy of the oxygen molecule. Similarly, the H and  $\text{H}_2\text{O}$  adsorption energies are evaluated using the formula  $E_{\text{ads}}(X) = 1/2[E_{\text{TOT}}(2X) - E_{\text{TOT}} - 2E(X)]$  (with  $X = \text{H}$  or  $\text{H}_2\text{O}$ ), where  $E_{\text{TOT}}(X)$  refers to the DFT total energies of the symmetric slab containing two H adatoms or two water molecules, whereas  $E(X)$  represents the DFT energies of the isolated H atom or  $\text{H}_2\text{O}$  molecule.

The energy barriers for the water dissociation processes were determined via the climbing image NEB (CI-NEB) method,<sup>49</sup> which is designed to compel one of the intermediate states near the transition point to climb up along the reaction coordinate to reach the highest saddle point, leading to an evaluation of the energy barrier that is more accurate than that of the regular NEB. Because of the computational load, we adopted 4–8 images connecting two subsequent minima of the potential-energy surface for determining the minimum energy path. The whole path was considered to be converged when the residual forces acting on the individual images dropped below the threshold of  $0.05 \text{ eV} \text{\AA}^{-1}$ . For the NEB calculations we did not include dispersion corrections on top of DFT, as it has been demonstrated that these have little impact on the activation energy.<sup>50</sup>

### 3. RESULTS

**3.1. Scanning Tunneling Microscopy.** Figure 2a shows an empty-states STM image of the  $\text{SrTiO}_3(110)$  surface after exposure to atomic hydrogen. The bright stripes along the  $[1\bar{1}0]$  direction correspond to the  $\text{Ti}_{\text{III}}$  and  $\text{Ti}_{\text{II}}$  atoms in the six-membered rings, located in tetrahedral units that connect to the  $\text{SrTiO}_3$  substrate below by sharing corners. The ridges are separated by a dark trench originating from the tetrahedra in the 10-membered rings, which share edges with the  $\text{SrTiO}_3$  underneath (Figure 1a). Each stripe contains two or three bright rows of periodic dots for the  $(4 \times 1)$  or  $(5 \times 1)$  reconstruction, respectively.<sup>21</sup> On top of the stripes, two types of bright protrusions are observed (labeled by red and white arrows). Sr adatoms, which are part of the  $(4 \times 1)$  antiphase domain structure,<sup>27</sup> are labeled with red arrows. In agreement with the DFT calculations<sup>27</sup> they are adsorbed in the middle of the six-membered rings, i.e., centered on the bright  $(4 \times 1)$  stripes. The Sr adatoms have an apparent height of  $\sim 240 \text{ pm}$ . (Quoted here and in the following are typical values for the apparent heights observed for an STM sample bias of  $+2.3 \text{ V}$  and a tunneling current of  $0.1 \text{ nA}$ . However, note that the apparent height also depends on the tip state.)

It is well-accepted that atomic hydrogen preferentially adsorbs on the surface oxygen atoms, forming hydroxyl groups.<sup>51–54</sup> In our case, the hydroxyl groups (labeled with white arrows in Figure 2a) have an apparent height of  $\sim 130 \text{ pm}$ , which is less than that of the Sr adatoms. The OH groups appear preferentially at the sides of both the  $(4 \times 1)$  and the  $(5 \times 1)$

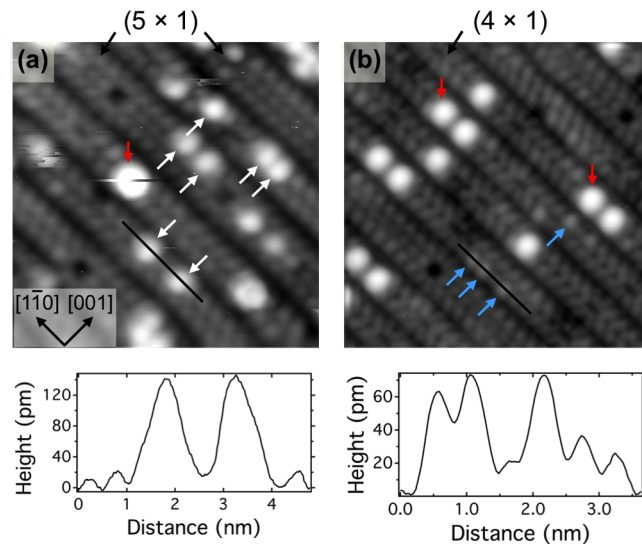


**Figure 2.** STM images (image size  $9 \times 9 \text{ nm}^2$ , sample bias  $+2.3 \text{ V}$ , tunneling current  $0.1 \text{ nA}$ ) of the  $\text{SrTiO}_3(110)$  surface. The surface exhibits an overall  $(4 \times 1)$  reconstruction; locally a few  $(5 \times 1)$  rows are apparent. (a) After exposure to atomic hydrogen and (b) after flashing the surface in panel (a) to  $\sim 300 \text{ }^\circ\text{C}$ . Sr adatoms, hydroxyls, and oxygen vacancies appear in various levels of brightness and are labeled by red, white, and blue arrows, respectively. The line profiles in the lower panels were taken at the lines shown in the STM images.

$\times 1$ ) stripes. DFT calculations (below) show that atomic hydrogen prefers to adsorb at the  $\text{O}_3$  site (Figure 1), and the resulting simulated STM image is consistent with experimental results.<sup>21</sup> It should be noted that we also observed indications of H interaction with Sr adatoms; for example, note the streaky appearance of the extra-bright Sr atom in Figure 2a that indicates the presence of an adsorbate.

After the hydroxylated surface was flashed to about  $300 \text{ }^\circ\text{C}$ , less bright protrusions with an apparent height of  $\sim 70 \text{ pm}$  appear (blue arrows in Figure 2b). From TPD and STM experiments it is often observed that molecular water desorbs from hydroxylated oxide surfaces upon flash-annealing.<sup>37,53,54</sup> Indeed, from a prior TPD study a similar conclusion was drawn for the  $\text{SrTiO}_3(001)$  surface.<sup>13</sup> It was observed that molecular water desorbs above  $100 \text{ }^\circ\text{C}$  on the hydroxylated  $\text{SrTiO}_3(001)$  surface.<sup>13</sup> Therefore, it is reasonable to attribute the less bright protrusions to  $\text{V}_O$ 's. The  $\text{V}_O$ 's sit also at the side of the  $(4 \times 1)$  stripes, similar to the hydroxyls. These results agree very well with the preference for a  $\text{V}_O$  at the  $\text{O}_3$  site in DFT calculations as shown in the following and in ref 21.

Figure 3a shows an LT-STM image of the  $\text{SrTiO}_3(110)$  surface after exposure to 0.3 langmuir water at  $110 \text{ K}$ . Bright features with an apparent height of  $\sim 80 \text{ pm}$ , labeled with green arrows, appear in the trenches between stripes. These features are different from the  $\text{V}_O$ 's and hydroxyls in Figure 2. From TPD measurements on the  $\text{SrTiO}_3(001)$  surface, molecular water starts to desorb around  $200\text{--}260 \text{ K}$  at low exposure ( $< 1$  langmuir), while weakly bound and multilayer water desorbs below  $200 \text{ K}$  upon further exposure.<sup>13</sup> We attribute the features in Figure 3a to molecular water that is located at the cation sites at low exposure. From the DFT calculations shown below, molecular water preferentially adsorbs at the  $\text{Ti}_{\text{I}}$  site in the 10-membered rings on the  $\text{SrTiO}_3(110)\text{--}(4 \times 1)$  surface (Figure 1b), consistent with the experimental observations.

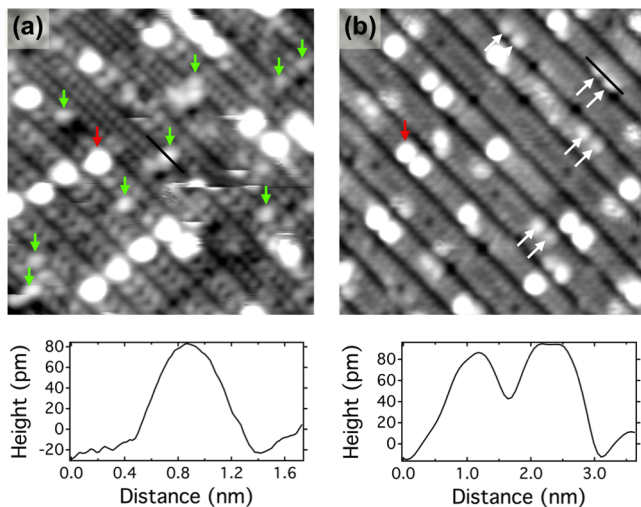


**Figure 3.** STM images ( $18 \times 18 \text{ nm}^2$ , 2.1 V, 0.1 nA) of the  $\text{SrTiO}_3(110)$ -(4  $\times$  1) surface after exposure to (a) 0.3 langmuir water at 110 K, imaged at 78 K; (b) 3 langmuir water at RT, imaged at RT. Green and white arrows point to molecular water and hydroxyl pairs, respectively. As in Figure 2 the red arrows point out single Sr adatoms. The line profiles in the lower panels were taken at the lines shown in the STM images.

After the surface is dosed with 3 langmuir water at RT, bright features with an apparent height similar to hydroxyls formed on the H-exposed surface appear at the sides of both the (4  $\times$  1) and (5  $\times$  1) stripes (Figure 3b), indicating hydroxyl formation after dosing with water at RT. In addition to single hydroxyls, hydroxyl pairs are also observed on the surface, again labeled by white arrows in Figure 3b. These pairs are likely due to the dissociation of water at the  $\text{V}_\text{O}$ 's. In Figure 3b the distance between these hydroxyl pairs is two unit cells along the [110] direction. Here the saturation coverage of hydroxyls is approximately 0.01 ML (1 ML =  $4.64 \times 10^{14}$  atoms  $\text{cm}^{-2}$  relative to the  $\text{SrTiO}_3(110)$ -(1  $\times$  1) unit cell), suggesting a surface  $\text{V}_\text{O}$  density of half that value. Further increasing the water dosage up to 50 langmuir does not introduce more hydroxyls on the surface, and no indication of molecular water is observed. We conclude that water dissociates only on the  $\text{V}_\text{O}$ 's whereas it neither adsorbs nor dissociates on the stoichiometric surface at RT.

**3.2. Photoemission Spectroscopy.** Figure 4a shows photoemission spectra of the valence band region of differently treated  $\text{SrTiO}_3(110)$  surfaces. The valence band of the clean

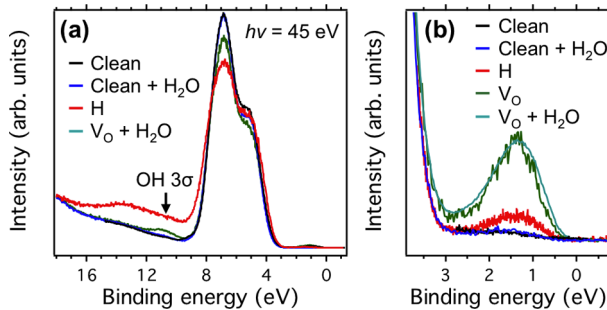


**Figure 4.** Comparison of valence band photoemission spectra of the clean surface (black), after exposure to water (blue), atomic hydrogen (red), of a surface with oxygen vacancies (green), and after exposure to water (cyan). All spectra were taken at RT.

surface shows mainly O 2p-derived features. By linearly extrapolating the onset of the spectra, the valence band maximum (VBM) is determined to be located at 3.2 eV below the Fermi level ( $E_\text{F}$ ), in agreement with the Nb-doped n-type sample and a reported band gap of 3.2 eV for  $\text{SrTiO}_3$ .<sup>55</sup> For the clean surface no states are observed in the band gap region (see Figure 4b), indicating that Nb dopants do not induce in-gap states. This is consistent with the picture that the band structure of lightly n-type doped samples can be well-described by a simple rigid band shift.<sup>57</sup>

After the clean surface is dosed with up to 240 langmuir water at RT, the valence band spectrum does not change compared to that of the clean surface (see Figure 4a,b). For molecularly adsorbed water one would expect features related to its 1b<sub>2</sub>, 3a<sub>1</sub>, and 1b<sub>1</sub> orbitals.<sup>58</sup> On the other hand, an OH 3σ state as well as in-gap states can be observed when dissociative adsorption occurs.<sup>6–10,59</sup> In experiments on as-dosed samples, we did not observe any features related to molecular and dissociative water, in agreement with the conclusion of a rather unreactive surface drawn on the basis of our STM results.

After atomic hydrogen dosing, an in-gap state with a binding energy of 1.3 eV is observed (see the red curve in Figure 4b), as well as a feature below the O 2p valence band. Partially this feature can be assigned to the OH 3σ state, which is located at 10.8 eV.<sup>60</sup> At first sight, the higher binding energy features could be associated with water 1b<sub>2</sub> and 3a<sub>1</sub> states. However, water does not adsorb on the clean surface at RT, as shown in our STM measurements. Furthermore, no features were observed related to molecular water from the O 1s core-level spectrum for the H-exposed surface (Figure 5). Instead, STM indicates that H interacts with the Sr adatoms. We tentatively attribute the higher binding energy features to states related to Sr–OH species.<sup>11,12</sup>

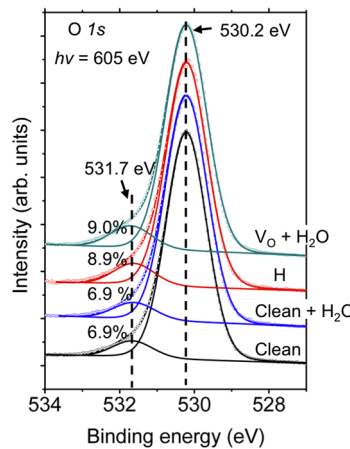


**Figure 5.** Comparison of O 1s core-level XPS spectra of the clean surface (black), after exposure to water (blue) and atomic hydrogen (red), and the surface with oxygen vacancies exposed to water (cyan). All spectra were taken at RT.

An in-gap state appears after creating  $\text{V}_\text{O}$ 's on the clean surface by exposing the surface to intense synchrotron radiation. After exposure to synchrotron light a similar in-gap state and related two-dimensional electron gas were observed on  $\text{SrTiO}_3(001)$  and other perovskite surfaces,<sup>57,61,62</sup> as well as on  $\text{TiO}_2$  surfaces.<sup>54</sup> We find that the in-gap state can be quenched by exposure to  $\text{O}_2$  at RT, supporting the conclusion that it arises from  $\text{V}_\text{O}$ 's.<sup>57</sup>

When the surface with  $V_O$ 's is exposed to 1.2 langmuir water at RT, the in-gap state hardly changes as shown in Figure 4b. However, a well-defined OH  $3\sigma$  state with a binding energy of 10.8 eV is observed (see the cyan curve in Figure 4a), which indicates water dissociation and formation of hydroxyls. It is well-known that the presence of hydroxyls results in an in-gap state similar to  $V_O$ 's.<sup>58</sup> This supports the conclusion that water dissociates on the reduced surface.

Similar conclusions are drawn from the corresponding O 1s core-level photoemission spectra (Figure 5). The O 1s spectrum obtained on the clean surface shows a slightly asymmetric peak shape with the main peak located at 530.2 eV and a small shoulder at a higher binding energy of 531.7 eV. The spectrum does not change after dosing water on the clean surface at RT. After atomic hydrogen and water dosing on the reduced surface, the ratio increases slightly. This result is consistent with observations on the titania surface.<sup>63–65</sup>

**3.3. Electronic Structure Calculations.** To complement the photoemission spectra and achieve an understanding of the electronic properties of the defective and hydroxylated surface as compared to the clean ( $4 \times 1$ ) surface, we have determined the most stable configurations and computed their density of states (DOS). By comparing the energies of all possible inequivalent configurations, we determined the most favorable site for the formation of a  $V_O$  and for hydrogen adsorption.

The results, collected in Table 1, show that O3 has the lowest  $V_O$  formation energy, in agreement with a recent first-

**Table 1. Oxygen Vacancy Formation Energy  $E_f(V_O)$  and Hydrogen Adsorption Energy  $E_{ads}(H)$  for Different Oxygen Sites Obtained with the PBE Functional<sup>a</sup>**

	O1	O2	O3	O4	O5
$V_O$ formation energy (eV)	6.43 (0.83)	5.95 (0.35)	5.60 (0.0)	5.68 (0.08)	5.76 (0.16)
H adsorption energy (eV)	1.79 (−0.40)	1.93 (−0.26)	2.19 (0.0)	2.16 (−0.03)	1.62 (−0.57)

<sup>a</sup>Oxygen sites are named according to the labeling given in Figure 1b. Numbers in parentheses refer to the relative energy with respect to the most stable configuration. For geometries of adsorbed H, see the Supporting Information.

principles study<sup>21</sup> and consistent with our STM measurements (Figure 2b). In addition, the O3 site is the most favorable hydrogen adsorption site, with an adsorption energy of 2.19 eV. The most stable hydroxyl is characterized by an O–H bond length of 0.983 Å, slightly larger than that of a free OH group (0.97 Å), and a 45.1° angle with respect to the surface normal.

We have calculated the DOS of the most favorable oxygen-defective and hydroxylated surfaces. The results are compared to the clean ( $4 \times 1$ ) surface in Figure 6. Given the well-known drawbacks of standard (local and semilocal) DFT functionals in predicting the correct electronic ground state of strongly correlated electron systems and in describing electron localization effects, we have computed the DOS by means of the PBE+U method,<sup>66</sup> using an effective on-site Coulomb repulsion  $U_{eff} = 4.6$  eV for the Ti d states, a choice in line with previous studies.<sup>67</sup> The most relevant feature of the  $V_O$  case is the appearance of a midgap state right above the valence band maximum, in agreement with the photoemission data. This state originates from the  $Ti^{3+}$  atoms adjacent to the  $V_O$ , which locally trap the extra electrons created by the  $V_O$ . The

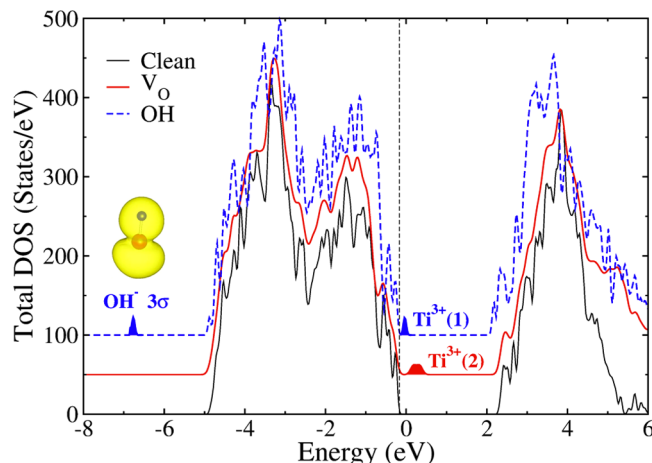


**Figure 6.** PBE+U valence and conduction band density of states of the clean  $SrTiO_3(110)$ -( $4 \times 1$ ) surface (thin black line) and the reduced surface with an oxygen vacancy (red solid line) and hydroxyl species (dashed blue line). All spectra are aligned with respect to their valence-band maxima. The  $Ti^{3+}$  midgap states (both singly,  $Ti^{3+}$  (1), and doubly,  $Ti^{3+}$  (2) occupied) as well as the  $OH^-$   $3\sigma$  states are highlighted with a colored background.

adsorption of one OH group leads to the formation of only one  $Ti^{3+}$  and to the emergence of a feature at about −7 eV below the VBM. This feature is attributed to the  $OH^-$   $3\sigma$  bonding state, as shown in the inset of Figure 6. This picture is reminiscent of the one found for the rutile  $TiO_2(110)$  surface.<sup>68–70</sup>

**3.4. DFT Calculations: Interaction with  $H_2O$ .** To elucidate the adsorption of water on the  $SrTiO_3(110)$ -( $4 \times 1$ ) surface and to examine the role of  $V_O$ 's, we have performed NEB calculations. One important question is whether the water is predicted to adsorb molecularly or dissociatively on the  $SrTiO_3(110)$  surface. To answer this question we have investigated the energetics of different adsorption configurations at low coverage, both in molecular and dissociated form, as well as the dissociation energy barriers and pathways among the different configurations. We first focus on the interaction between water and the clean ( $4 \times 1$ ) surface, and then we discuss the results obtained for the reduced surface.

**3.4.1. Ideal Surface +  $H_2O$ . Molecular Adsorption.** Our first concern is to identify locally stable molecular  $H_2O$  configurations. We have scrutinized several possible adsorption sites at a coverage of 1/8 ML (one  $H_2O$  molecule per ( $4 \times 2$ ) unit cell).

The most favorable adsorption site is located in the 10-membered rings near  $Ti_l$ , as shown in the insets of Figure 7. The distance between  $Ti_l$  and the water oxygen atom ( $O_W$ ) is found to be 2.341, 2.325, and 2.311 Å with the PBE, DFT-D2, and vdW-DFT functionals, respectively. The corresponding water adsorption energies  $E_{ads}(H_2O)$  are −0.716, −1.014, and −1.073 eV, respectively. As expected, the van der Waals correction substantially increases the magnitude of the adsorption energy, although the geometries are similar to those of the standard PBE case. Moreover, the other configurations considered are less stable by 0.15–0.5 eV. Both the H– $O_W$  bond length (1.00 Å) and the H– $O_W$ –H bond angle (106°) are almost identical to the corresponding values in the free water molecule (0.985 Å and 104.96°, respectively). We also evaluated adsorption energies at the experimental condition (300 K and  $10^{-9}$  bar) within the

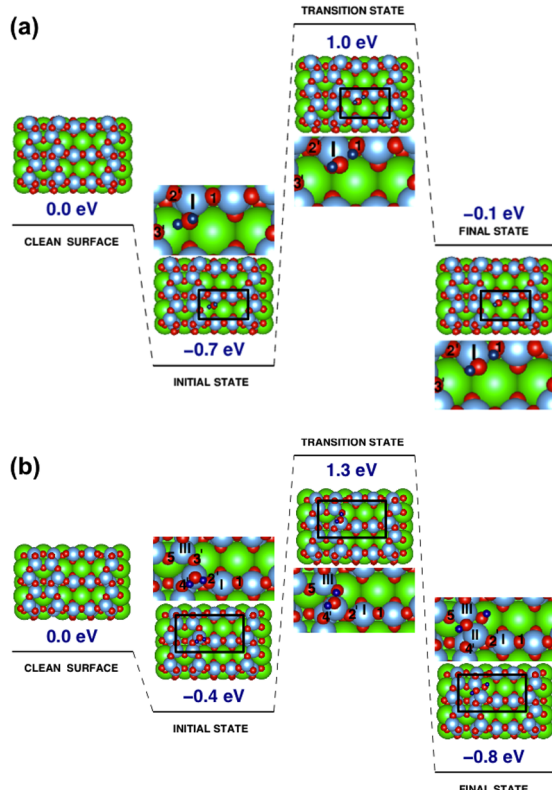


**Figure 7.** Potential-energy profiles for the dissociative adsorption of  $\text{H}_2\text{O}$  molecule on the ideal, nondefective  $\text{SrTiO}_3(110)\text{-(}4\times 1)$  surface. Pathways were evaluated for (a) the most favorable configuration for molecular adsorption and (b) the most favorable configuration for dissociative adsorption. The energy zero corresponds to  $\text{H}_2\text{O}$  in the gas phase, far away from the surface. For each state the corresponding optimized structures are shown as insets in wide and zoomed view.

framework of “ab initio thermodynamics”.<sup>71,72</sup> The corresponding values are +0.482, 0.184, and 0.125 eV with the PBE, DFT-D2, and vdW-DFT functionals, respectively. The positive value indicates that water does not adsorb on the ideal surface, in agreement with experiment.

**Dissociative Adsorption.** To explore the dissociative configuration (coadsorption of H and OH species), which serves as a basis for studying the water dissociation process, we assumed that the OH species preferentially adsorbs on the Ti atom and the H atom on the neighboring or next-neighboring surface O atoms. This assumption is reasonable as no local minimum corresponding to an adsorption at the surface Ti site was found for the H atom.

Most of the dissociative adsorption configurations we explored are unstable (i.e., with positive adsorption energy), or relax to the molecular pattern (see Supporting Information). We established only five stable or metastable dissociative patterns with negative or zero adsorption energy. As mentioned

before, here we performed the calculations with the PBE functional because application of DFT-D2 and vdW-DFT does not alter the adsorption sequence or geometries. The computed adsorption energy for the most stable pattern is  $-0.779$  eV, about 60 meV more stable than the molecular adsorption case. In this configuration (Figure 7b), the OH species anchors on the bridge site between the two Ti surface atoms ( $\text{Ti}_{\text{II}}$  and  $\text{Ti}_{\text{III}}$ ), while the atom  $\text{O}_3$ , bonded to another H atom, shifts downward because of the electrostatic potential repulsion; this results in two 5-fold coordinated Ti atoms.

On the basis of the computed adsorption energies alone we cannot unambiguously determine whether water molecules are predicted to adsorb molecularly or dissociatively on the  $\text{SrTiO}_3(110)\text{-(}4\times 1)$  surface. We have conducted a series of CI-NEB calculations in order to model the dynamics (see Supporting Information).

**Dissociative Reaction.** We have determined the energy barrier for the water dissociation processes from the most stable molecular adsorption state (initial state) to the geminate dissociative state (final state) (Figure 7a) as well as from a metastable adsorption state to the most favorable dissociative state (Figure 7b) by using the CI-NEB method. This procedure allows us to find the minimum energy reaction paths. The transition barrier for the  $\text{H}_2\text{O}$  to dissociate on the  $\text{SrTiO}_3(110)\text{-(}4\times 1)$  surface is rather large ( $>1.7$  eV), much higher than the adsorption energies of both the molecularly or dissociated state, making spontaneous dissociation an unlikely process. This clearly shows that the  $\text{H}_2\text{O}$  molecule is not predicted to dissociate on the defect-free surface, in agreement with the experimental observations.

**3.4.2. Reduced Surface +  $\text{H}_2\text{O}$ .** As mentioned in the experimental section, significant amounts of hydroxyls are found on the  $\text{SrTiO}_3(110)\text{-(}4\times 1)$  surface with  $\text{V}_\text{O}$ 's after water dosing. This suggests that the oxygen deficient surface is active with respect to water dissociation.

The water adsorption energies computed within PBE, DFT-D2 and vdW-DFT are listed in Table 2. All three methods yield very similar values of  $-1.7$  eV, substantially larger (by about 1 eV) than those on the stoichiometric, nondefective surface. Adapting the correction based on “ab initio thermodynamics” as mentioned above, delivers substantial adsorption energy (about  $-0.5$  eV) at the experimental conditions, suggesting the adsorption of water on the defective surface is clearly favorable. Van der Waals interactions do not play a significant role, which is suggestive of a primarily chemisorption process.

Considering that the three different methods also deliver a quantitatively similar description of the structural characteristics (see Table 2), we will focus only on the PBE results in the following. The structural model of the optimized initial configuration is provided in Figure 8. In the optimized structure, the  $\text{H}_2\text{O}$  molecule is slightly tilted toward one of the 3-fold-coordinated Ti atoms near the  $\text{V}_\text{O}$ , forming two asymmetric  $\text{Ti}-\text{O}_\text{W}$  bonds of 2.107 and 3.090 Å. One of the

**Table 2.** Calculated Water Adsorption Energies  $E_{\text{ads}}(\text{H}_2\text{O})$ , Bond Lengths ( $\text{O}_\text{W}$  and  $\text{O}_\text{S}$  Denote O Atoms in the Water Molecule and Surface, Respectively), and  $\text{H}-\text{O}_\text{W}-\text{H}$  Angles for Molecular Adsorption Configurations on the Defective Surface, Calculated with Different Functionals

functional	$E_{\text{ads}}(\text{H}_2\text{O})$ (eV)	$\text{Ti}-\text{O}_\text{W}$ (Å)	$\text{H}-\text{O}_\text{W}$ (Å)	$\text{H}-\text{O}_\text{S}$ (Å)	$\text{H}-\text{O}_\text{W}-\text{H}$ (degrees)
PBE	-1.732	2.107, 3.090	1.055, 0.985	1.571	109.22
DFT-D2	-1.857	2.102, 3.061	1.057, 0.985	1.560	109.31
vdW-DFT	-1.727	2.098, 3.167	1.059, 0.987	1.552	109.35

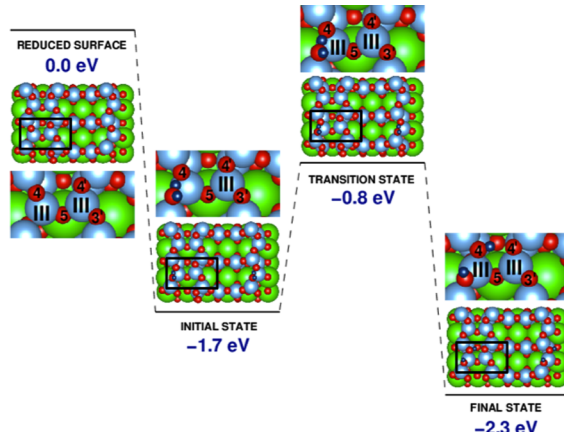


**Figure 8.** Potential-energy profile for the reaction of an adsorbed  $\text{H}_2\text{O}$  molecule at the defective  $\text{SrTiO}_3(110)$ - $(4 \times 1)$  surface. The energy zero corresponds to the  $\text{H}_2\text{O}$  in the gas phase, far away from the surface.

$\text{H}-\text{O}_\text{W}$  bonds in the adsorbed water molecule points toward the  $\text{O}4$  atom, forming an  $\text{H}$ -bond with a bond length of 1.571 Å, in turn slightly enlarging the molecular  $\text{H}-\text{O}_\text{W}$  bond length to 1.055 Å. The second  $\text{H}$  remains free, connected to the  $\text{O}_\text{W}$  with the corresponding  $\text{H}-\text{O}_\text{W}$  bond length (0.985 Å).

As mentioned above, we primarily focus on the original geminate dissociative states. The OH species occupies the  $\text{O}3$  vacancy site, with the remaining  $\text{H}$  atom anchored to the neighboring  $\text{O}4$  atom (see inset in Figure 8). The resulting  $\text{O}4-\text{H}$  is nearly flat-lying and is  $\text{H}$ -bonded with the adjacent  $\text{O}4'$  surface oxygen atom. This structural and chemical environment results in a large adsorption energy of 2.28 eV. This is already a strong indication that the water molecule is preferentially adsorbed dissociatively rather than molecularly. However, exothermicity is a necessary, but not sufficient, condition for dissociation. To gain more insight into the dissociative adsorption process we have conducted NEB calculations for the energy barrier. The resulting energy profile for the dissociation pathway in Figure 8 shows an energy barrier at the transition state of 0.9 eV. This barrier is significantly lower than the corresponding values (1.7 eV) obtained on the ideal surface, clearly indicating that  $\text{V}_\text{O}$ 's strongly facilitate water dissociation. This is again in excellent agreement with experimental observations, which reveal that water interacts with  $\text{V}_\text{O}$ 's, forming two hydroxyl groups on the surface. Similar energy pathways for the dissociative process were also found for the defective surface with an  $\text{O}4$  vacancy, which is characterized by an exothermic energy of 1.4 eV and a slightly larger barrier of 1.1 eV. Given the theoretical and experimental results above, it is clear that  $\text{V}_\text{O}$ 's facilitate water dissociation on the  $\text{SrTiO}_3(110)$  surface and the barriers are low enough for this process to happen at room temperature or slightly above RT.

#### 4. DISCUSSION

Our DFT calculations show that the  $\text{V}_\text{O}$ 's are preferentially created at the  $\text{O}3$  site in the six-membered ring of the  $(4 \times 1)$  reconstruction, which is also the most favorable site to form OH. This is in excellent agreement with the experimental STM images (Figure 2). Moreover, the water tends to adsorb molecularly at the  $\text{Ti}_\text{l}$  site in the 10-membered ring, where it appears as bright protrusions between the stripes in the STM images at low temperature (Figure 3a).

The situation is different when water is dosed in the presence of  $\text{V}_\text{O}$ 's. Both the experimental and theoretical results unequivocally show that water dissociates spontaneously at the  $\text{V}_\text{O}$ 's at finite temperatures. In STM the two OH groups resulting from a dissociated water molecule were observed far from each other. The DFT-calculated energy barrier for the direct  $\text{H}$  diffusion is  $\sim 1.35$  eV, indicating that the direct hopping is not possible at RT. Possibly these OH groups are driven apart via the water-assisted mechanism reported in refs 73 and 74.

Overall, the ideal, nondefective  $\text{SrTiO}_3(110)$ - $(4 \times 1)$  surface is remarkably inert toward water adsorption, while the  $\text{V}_\text{O}$ 's facilitate bonding and dissociation of water. Moreover,  $\text{V}_\text{O}$ 's created on the  $\text{SrTiO}_3(110)$  surface are metastable and inclined to diffuse to subsurface sites as suggested in previous studies.<sup>21</sup> Therefore, under real-world conditions we expect vacancy-mediated adsorption and dissociation to be rare on this surface.

As stated in the Introduction,  $\text{SrTiO}_3(110)$  is a polar surface, consisting of alternating  $(\text{SrTiO})^{4+}$  and  $(\text{O}_2)^{4-}$  planes in the bulk. While an uncompensated polar surface is unstable and chemically active, our results indicate that in this case compensating polarity with the reconstruction network is very efficient in creating an inert surface. The most peculiar structural feature of the reconstruction is the presence of the  $\text{TiO}_4$  tetrahedra on the top layer. Interestingly, the  $\text{Ti}_\text{l}$ -tetrahedra (edge-sharing with the substrate) in the 10-membered rings are reminiscent of a similar configuration at the reconstructed anatase  $\text{TiO}_2(001)$ - $(1 \times 4)$  surface,<sup>28</sup> which contains a distorted  $\text{TiO}_4$  tetrahedron. It was demonstrated that water dissociates spontaneously on the ridge of this reconstructed surface in theoretical and experimental studies.<sup>32,33</sup> In fact, the anatase  $\text{TiO}_2(001)$  surface is considered to be the most active facet in photocatalytic reactions.<sup>34</sup> An analysis of our results gives insights as to why the  $\text{TiO}_4$  tetrahedra are so inert in the case of  $\text{SrTiO}_3(110)$ - $(4 \times 1)$ .

**Electronic Aspects.** While excess electrons located at the energies near the band gap of reducible oxide surfaces are generally connected with a high reactivity,<sup>75</sup> the clean  $\text{SrTiO}_3(110)$ - $(4 \times 1)$  surface has no in-gap states in both experiment and theory. In fact, an analysis of the layer-resolved DOS (not shown) indicates that the top layer has a band gap that is slightly larger than that of the  $\text{SrTiO}_3$  layers underneath. In spite of the 4-fold coordination in this tetrahedral configuration, the  $\text{Ti}$  atom should not be considered undersaturated. The  $\text{Ti}$  atom hybridizes with the four surrounding oxygen atoms, forming strong covalent bonds with a short bond length, which lead to the relatively large band gap. Experimental and theoretical results also show that the  $\text{Ti}$  valence is  $4^+$  and no in-gap state is present on the anatase  $\text{TiO}_2(001)$ - $(1 \times 4)$  surface.<sup>28,76</sup> Thus, while explaining our inert  $\text{SrTiO}_3(110)$ - $(4 \times 1)$  surface, the electronic structure provides no argument for the supposedly reactive  $\text{TiO}_4$  tetrahedra on anatase.

Interestingly, similar tetrahedrally coordinated  $\text{TiO}_4$  units are present on the  $\text{TiO}_2(110)$ - $(1 \times 2)$  surface, forming one-dimensional  $\text{Ti}_2\text{O}_3$  rows.<sup>29</sup> Because of the presence of  $\text{Ti}^{3+}$  species, the  $\text{TiO}_2(110)$ - $(1 \times 2)$  surface is proposed to be chemically active, as demonstrated by reacting with  $\text{NO}$ .<sup>77</sup> It would be interesting to test whether this surface is also reactive for water dissociation.

**Structural Aspects.** What is needed for strong water interaction are freely accessible acidic sites and a neighboring O atom that can act as a Brønsted base (proton acceptor). In our case, the  $\text{TiO}_4$  tetrahedron is quite regular: the bond length

ranges from 1.826 to 1.896 Å, with an O–Ti–O bond angle range of 92.82–123.08°. The acidic Ti sites are significantly recessed into the surface compared to the surrounding oxygen atoms, making them inaccessible and nonreactive. In contrast, on the anatase  $\text{TiO}_2(001)$ -(1 × 4) reconstructed surface, the  $\text{TiO}_4$  tetrahedron is very distorted; the bond length along the [100] direction consists of alternating long (2.134 Å) and short (1.831 Å) Ti–O bonds, while the bonds along the [010] directions are identical (1.805 Å). The O–Ti–O bond angles along the [100] and [010] directions are 145.15° and 104.76°, respectively,<sup>32</sup> leading to the exposure of the Ti atom as an active acidic site. Furthermore, and at variance with what was found for  $\text{SrTiO}_3(110)$ -(4 × 1), the distorted  $\text{TiO}_4$  tetrahedron on the anatase  $\text{TiO}_2(001)$ -(1 × 4) surface forms a quasi-one-dimensional row along the [100] direction. This flexible framework provides freedom of relaxation and facilitates the water dissociation. At the  $\text{SrTiO}_3(110)$ -(4 × 1) surface, the two-dimensional nesting of the 6- and 10-membered rings is more rigid, which contributes to its inertness.

A similar two-dimensional reconstructed overlayer consisting of corner-sharing  $\text{TiO}_4$  regular tetrahedra has been established on the rutile  $\text{TiO}_2(100)$ -c(2 × 2) surface.<sup>31</sup> From the present results, we would expect this reconstructed surface also to be relatively inert; it would be interesting to test this prediction.

## 5. SUMMARY AND CONCLUSION

We have performed a systematic study of water interaction with the two-dimensional titania overlayer consisting of  $\text{TiO}_4$  tetrahedra on the  $\text{SrTiO}_3(110)$ -(4 × 1) surface with and without oxygen vacancies. We found that water dissociates on the oxygen vacancies, in line with many other oxide surfaces. We also found the two-dimensional, tetrahedrally coordinated  $\text{TiO}_4$  overlayer to be remarkably inert, in contrast to the one-dimensional, tetrahedrally coordinated  $\text{TiO}_4$  units at the anatase  $\text{TiO}_2(001)$ -(1 × 4) surface. The weak water adsorption on this surface stems from the regular tetrahedra and the two-dimensional rigid network as well as its insulating electronic structure. Recently,  $\text{TiO}_4$  tetrahedra have emerged as a common building block on many Ti-containing oxides surfaces. We expect that our conclusions of an inert two-dimensional top layer should also apply to these newly discovered surfaces.

## ■ ASSOCIATED CONTENT

### Supporting Information

H adsorption, molecular and dissociative  $\text{H}_2\text{O}$  adsorption configurations and energies on ideal surface, and energy diagrams for dissociation of  $\text{H}_2\text{O}$ . This material is available free of charge via the Internet at <http://pubs.acs.org>.

## ■ AUTHOR INFORMATION

### Corresponding Author

\*E-mail: diebold@iap.tuwien.ac.at. Phone: +43-1-58801-13425.

### Notes

The authors declare no competing financial interest.

## ■ ACKNOWLEDGMENTS

This work has been supported by the Austrian Science Fund (FWF) under Project F45 and the ERC Advanced Research Grant, OxideSurfaces. E.M. acknowledges support from the FWF under Project W1243 (Solids4Fun). All DFT calculations were performed at the Vienna Scientific Cluster (VSC-2).

Valuable discussions with Annabella Selloni and Laurence Marks are gratefully acknowledged.

## ■ REFERENCES

- Mavroides, J.; Kafalas, J.; Kolesar, D. Photoelectrolysis of Water in Cells with  $\text{SrTiO}_3$  Anodes. *Appl. Phys. Lett.* **1976**, *28*, 241–243.
- Wrighton, M. S.; Ellis, A. B.; Wolczanski, P. T.; Morse, D. L.; Abrahamson, H. B.; Ginley, D. S. Strontium Titanate Photoelectrodes. Efficient Photoassisted Electrolysis of Water at Zero Applied Potential. *J. Am. Chem. Soc.* **1976**, *98*, 2774–2779.
- Townsend, T. K.; Browning, N. D.; Osterloh, F. E. Nanoscale Strontium Titanate Photocatalysts for Overall Water Splitting. *ACS Nano* **2012**, *6*, 7420–7426.
- Townsend, T. K.; Browning, N. D.; Osterloh, F. E. Overall Photocatalytic Water Splitting with  $\text{NiO}_x$ – $\text{SrTiO}_3$ —A Revised Mechanism. *Energy Environ. Sci.* **2012**, *5*, 9543–9550.
- Henrich, V. E.; Dresselhaus, G.; Zeiger, H. J. Chemisorbed Phases of  $\text{H}_2\text{O}$  on  $\text{TiO}_2$  and  $\text{SrTiO}_3$ . *Solid State Commun.* **1977**, *24*, 623–626.
- Ferrer, S.; Somorjai, G. A. UPS and XPS Studies of the Chemisorption of  $\text{O}_2$ ,  $\text{H}_2$  and  $\text{H}_2\text{O}$  on Reduced and Stoichiometric  $\text{SrTiO}_3(111)$  Surfaces; The Effects of Illumination. *Surf. Sci.* **1980**, *94*, 41–56.
- Webb, C.; Lichtensteiger, M. UPS/XPS Study of Reactive and Non-reactive  $\text{SrTiO}_3(100)$  Surfaces: Adsorption of  $\text{H}_2\text{O}$ . *Surf. Sci.* **1981**, *107*, L345–L349.
- Egdell, R. G.; Naylor, P. D. *Chem. Phys. Lett.* **1982**, *91*, 200–205.
- Cox, P. A.; Egdell, R. G.; Naylor, P. D. HREELS Studies of Adsorbates on Polar Solids: Water on  $\text{SrTiO}_3(100)$ . *J. Electron Spectrosc. Relat. Phenom.* **1983**, *29*, 247–252.
- Eriksen, S.; Naylor, P. D.; Egdell, R. G. The Adsorption of Water on  $\text{SrTiO}_3$  and  $\text{TiO}_2$ : A Reappraisal. *Spectrochim. Acta Mol. Spectrosc.* **1987**, *43*, 1535–1538.
- Brookes, N. B.; Thornton, G.; Quinn, F. M.  $\text{SrTiO}_3(100)$  Step Sites as Catalytic Centers for  $\text{H}_2\text{O}$  Dissociation. *Solid State Commun.* **1987**, *64*, 383–386.
- Brookes, N. B.; Quinn, F. M.; Thornton, G. The Involvement of Step and Terrace Sites in  $\text{H}_2\text{O}$  Adsorption on  $\text{SrTiO}_3(100)$ . *Phys. Scr.* **1987**, *36*, 711–714.
- Wang, L. Q.; Ferris, K. F.; Herman, G. S. Interactions of  $\text{H}_2\text{O}$  with  $\text{SrTiO}_3(100)$  Surfaces. *J. Vac. Sci. Technol., A* **2002**, *20*, 239–244.
- Wang, L.-Q.; Ferris, K. F.; Azad, S.; Engelhard, M. H. Adsorption of Water on (001) Surface of  $\text{SrTiO}_3$  and  $\text{SrZrO}_3$  Cubic Perovskites: Hybrid HF-DFT LCAO Calculations. *J. Phys. Chem. B* **2005**, *109*, 4507–4513.
- Baniecki, J. D.; Ishii, M.; Kurihara, K.; Yamanaka, K.; Yano, T.; Shinozaki, K.; Imada, T.; Kobayashi, Y. Chemisorption of Water and Carbon Dioxide on Nanostructured  $\text{BaTiO}_3$ – $\text{SrTiO}_3$ (001) Surfaces. *J. Appl. Phys.* **2009**, *106*, 054109.
- Guhl, H.; Miller, W.; Reuter, K. Water Adsorption and Dissociation on  $\text{SrTiO}_3(001)$  Revisited: A Density Functional Theory Study. *Phys. Rev. B* **2010**, *81*, 155455.
- Bonnell, D. A.; Garra, J. Scanning Probe Microscopy of Oxide Surfaces: Atomic Structure and Properties. *Rep. Prog. Phys.* **2008**, *71*, 044501.
- Russell, B.; Castell, M. Reconstructions on the Polar  $\text{SrTiO}_3(110)$  Surface: Analysis Using STM, LEED, and AES. *Phys. Rev. B* **2008**, *77*, 245414.
- Enterkin, J. A.; Subramanian, A. K.; Russell, B. C.; Castell, M. R.; Poeppelmeier, K. R.; Marks, L. D. A Homologous Series of Structures on the Surface of  $\text{SrTiO}_3(110)$ . *Nat. Mater.* **2010**, *9*, 245–248.
- Wang, Z.; Yang, F.; Zhang, Z.; Tang, Y.; Feng, J.; Wu, K.; Guo, Q.; Guo, J. Evolution of the Surface Structures on  $\text{SrTiO}_3(110)$  Tuned by Ti or Sr Concentration. *Phys. Rev. B* **2011**, *83*, 155453.
- Li, F.; Wang, Z.; Meng, S.; Sun, Y.; Yang, J.; Guo, Q.; Guo, J. Reversible Transition Between Thermodynamically Stable Phases with Low Density of Oxygen Vacancies on the  $\text{SrTiO}_3(110)$  Surface. *Phys. Rev. Lett.* **2011**, *107*, 036103.

- (22) Biswas, A.; Rossen, P. B.; Yang, C. H.; Siemons, W.; Jung, M. H.; Yang, I. K.; Ramesh, R.; Jeong, Y. H. Universal Ti-rich Termination of Atomically Flat  $\text{SrTiO}_3(001)$ , (110), and (111) Surfaces. *Appl. Phys. Lett.* **2011**, *98*, 051904.
- (23) Bottin, F.; Finocchi, F.; Noguera, C. Facetting and ( $n \times 1$ ) Reconstructions of  $\text{SrTiO}_3(110)$  Surfaces. *Surf. Sci.* **2005**, *574*, 65–76.
- (24) Noguera, C.; Goniakowski, J. Polarity in Oxide Ultrathin Films. *J. Phys.: Condens. Matter* **2008**, *20*, 264003.
- (25) Shin, J.; Nascimento, V. B.; Geneste, G.; Rundgren, J.; Plummer, E. W.; Dkhil, B.; Kalinin, S. V.; Baddorf, A. P. Atomistic Screening Mechanism of Ferroelectric Surfaces: An In Situ Study of the Polar Phase in Ultrathin  $\text{BaTiO}_3$  Films Exposed to  $\text{H}_2\text{O}$ . *Nano Lett.* **2009**, *9*, 3720–3725.
- (26) Wang, Z.; Feng, J.; Yang, Y.; Yao, Y.; Gu, L.; Yang, F.; Guo, Q.; Guo, J. Cation Stoichiometry Optimization of  $\text{SrTiO}_3(110)$  Thin Films with Atomic Precision in Homogeneous Molecular Beam Epitaxy. *Appl. Phys. Lett.* **2012**, *100*, 051602.
- (27) Wang, Z.; Li, F.; Meng, S.; Zhang, J.; Plummer, E. W.; Diebold, U.; Guo, J. Strain-Induced Defect Superstructure on the  $\text{SrTiO}_3(110)$  Surface. *Phys. Rev. Lett.* **2013**, *111*, 056101.
- (28) Lazzeri, M.; Selloni, A. Stress-Driven Reconstruction of an Oxide Surface: The Anatase  $\text{TiO}_2(001)-(1 \times 4)$  Surface. *Phys. Rev. Lett.* **2001**, *87*, 266105.
- (29) Blanco-Rey, M. M.; Abad, J. J.; Rogero, C. C.; Mendez, J. J.; Lopez, M. F. M.; Martin-Gago, J. A. J.; de Andres, P. L. P. Structure of Rutile  $\text{TiO}_2(110)-(1 \times 2)$ : Formation of  $\text{Ti}_2\text{O}_3$  Quasi-1D Metallic Chains. *Phys. Rev. Lett.* **2006**, *96*, 055502.
- (30) Marks, L. D.; Chiaramonti, A. N.; Tran, F.; Blaha, P. The Small Unit Cell Reconstructions of  $\text{SrTiO}_3(111)$ . *Surf. Sci.* **2009**, *603*, 2179–2187.
- (31) Warschkow, O.; Wang, Y.; Subramanian, A.; Asta, M.; Marks, L. D. Structure and Local-Equilibrium Thermodynamics of the  $c(2 \times 2)$  Reconstruction of Rutile  $\text{TiO}_2(100)$ . *Phys. Rev. Lett.* **2008**, *100*, 86102.
- (32) Gong, X.-Q.; Selloni, A.; Vittadini, A. Density Functional Theory Study of Formic Acid Adsorption on Anatase  $\text{TiO}_2(001)$ : Geometries, Energetics, and Effects of Coverage, Hydration, and Reconstruction. *J. Phys. Chem. B* **2006**, *110*, 2804–2811.
- (33) Blomquist, J.; Walle, L. E.; Uvdal, P.; Borg, A.; Sandell, A. Water Dissociation on Single Crystalline Anatase  $\text{TiO}_2(001)$  Studied by Photoelectron Spectroscopy. *J. Phys. Chem. C* **2008**, *112*, 16616–16621.
- (34) Yang, H. G.; Sun, C. H.; Qiao, S. Z.; Zou, J.; Liu, G.; Smith, S. C.; Cheng, H. M.; Lu, G. Q. Anatase  $\text{TiO}_2$  Single Crystals with a Large Percentage of Reactive Facets. *Nature* **2008**, *453*, 638–641.
- (35) Selçuk, S.; Selloni, A. Surface Structure and Reactivity of Anatase  $\text{TiO}_2$  Crystals with Dominant {001} Facets. *J. Phys. Chem. C* **2013**, *117*, 6358–6362.
- (36) Shaikhutdinov, S. S.; Freund, H.-J. H. Ultrathin Silica Films on Metals: The Long and Winding Road to Understanding the Atomic Structure. *Adv. Mater.* **2013**, *25*, 49–67.
- (37) Parkinson, G. S.; Novotný, Z.; Jacobson, P.; Schmid, M.; Diebold, U. Room Temperature Water Splitting at the Surface of Magnetite. *J. Am. Chem. Soc.* **2011**, *133*, 12650–12655.
- (38) Scheiber, P.; Riss, A.; Schmid, M.; Varga, P.; Diebold, U. Observation and Destruction of an Elusive Adsorbate with STM:  $\text{O}_2/\text{TiO}_2(110)$ . *Phys. Rev. Lett.* **2010**, *105*, 216101.
- (39) Nyholm, R.; Andersen, J. N.; Johansson, U.; Jensen, B. N.; Lindau, I. Beamline I311 at MAX-LAB: A VUV/Soft X-ray Undulator Beamline for High Resolution Electron Spectroscopy. *Nucl. Instrum. Methods Phys. Res. A* **2001**, *467*, 520–524.
- (40) Wang, Z.; Wu, K.; Guo, Q.; Guo, J. Tuning the Termination of the  $\text{SrTiO}_3(110)$  Surface by  $\text{Ar}^+$  Sputtering. *Appl. Phys. Lett.* **2009**, *95*, 021912.
- (41) Sutoh, A.; Okada, Y.; Ohta, S.; Kawabe, M. Cracking Efficiency of Hydrogen with Tungsten Filament in Molecular Beam Epitaxy. *J. Appl. Phys.* **1995**, *34*, L1379–L1382.
- (42) Kresse, G.; Hafner, J. *Ab Initio* Molecular Dynamics for Open-Shell Transition Metals. *Phys. Rev. B* **1993**, *48*, 13115–13118.
- (43) Kresse, G.; Furthmüller, J. Efficiency of Ab-Initio Total Energy Calculations for Metals and Semiconductors Using a Plane-Wave Basis Set. *Comput. Mater. Sci.* **1996**, *6*, 15–50.
- (44) Perdew, J. P.; Burke, K.; Ernzerhof, M. Generalized Gradient Approximation Made Simple. *Phys. Rev. Lett.* **1996**, *77*, 3865–3868.
- (45) Grimme, S. Accurate Description of van der Waals Complexes by Density Functional Theory Including Empirical Corrections. *J. Comput. Chem.* **2004**, *25*, 1463–1473.
- (46) Grimme, S. Semiempirical GGA-Type Density Functional Constructed with a Long-Range Dispersion Correction. *J. Comput. Chem.* **2006**, *27*, 1787–1799.
- (47) Grimme, S.; Antony, J.; Schwabe, T.; Mück-Lichtenfeld, C. Density Functional Theory with Dispersion Corrections for Supramolecular Structures, Aggregates, and Complexes of (Bio)Organic Molecules. *Org. Biomol. Chem.* **2007**, *5*, 741–758.
- (48) Klimeš, J.; Bowler, D. R.; Michaelides, A. Van der Waals Density Functionals Applied to Solids. *Phys. Rev. B* **2011**, *83*, 195131.
- (49) Henkelman, G.; Uberuaga, B. P.; Jónsson, H. A Climbing Image Nudged Elastic Band Method for Finding Saddle Points and Minimum Energy Paths. *J. Chem. Phys.* **2000**, *113*, 9901.
- (50) Sorescu, D. C.; Lee, J.; Al-Saidi, W. A.; Jordan, K. D.  $\text{CO}_2$  Adsorption on  $\text{TiO}_2(101)$  Anatase: A Dispersion-Corrected Density Functional Theory Study. *J. Chem. Phys.* **2011**, *134*, 104707.
- (51) Thiel, P. A.; Maday, T. E. The Interaction of Water with Solid Surfaces: Fundamental Aspects. *Surf. Sci. Rep.* **1987**, *7*, 211–385.
- (52) Henderson, M. A. The Interaction of Water with Solid Surfaces: Fundamental Aspects Revisited. *Surf. Sci. Rep.* **2002**, *46*, 1–308.
- (53) Weiss, W.; Ranke, W. Surface Chemistry and Catalysis on Well-Defined Epitaxial Iron-Oxide Layers. *Prog. Surf. Sci.* **2002**, *70*, 1–151.
- (54) Diebold, U. The Surface Science of Titanium Dioxide. *Surf. Sci. Rep.* **2003**, *48*, 53–229.
- (55) Cardona, M. Optical Properties and Band Structure of  $\text{SrTiO}_3$  and  $\text{BaTiO}_3$ . *Phys. Rev.* **1965**, *140*, A651–A655.
- (56) Cao, Y.; Wang, S.; Liu, S.; Guo, Q.; Wang, Z. Electronic Structures of the  $\text{SrTiO}_3(110)$  Surface in Different Reconstructions. *J. Chem. Phys.* **2012**, *137*, 044701.
- (57) Aiura, Y.; Hase, I.; Bando, H.; Yasue, T.; Saitoh, T.; Dessau, D. S. Photoemission Study of the Metallic State of Lightly Electron-Doped  $\text{SrTiO}_3$ . *Surf. Sci.* **2002**, *515*, 61–74.
- (58) Di Valentin, C.; Tilcock, A.; Selloni, A.; Beck, T. J.; Klust, A.; Batzill, M.; Losovyj, Y.; Diebold, U. Adsorption of Water on Reconstructed Rutile  $\text{TiO}_2(011)-(2 \times 1)$ :  $\text{Ti}=\text{O}$  Double Bonds and Surface Reactivity. *J. Am. Chem. Soc.* **2005**, *127*, 9895–9903.
- (59) Henrich, V. E.; Dresselhaus, G.; Zeiger, H. Surface Defects and the Electronic Structure of  $\text{SrTiO}_3$  Surfaces. *Phys. Rev. B* **1978**, *17*, 4908–4921.
- (60) D'Angelo, M.; Yukawa, R.; Ozawa, K.; Yamamoto, S.; Hirahara, T.; Hasegawa, S.; Silly, M.; Sirotti, F.; Matsuda, I. Hydrogen-Induced Surface Metallization of  $\text{SrTiO}_3(001)$ . *Phys. Rev. Lett.* **2012**, *108*, 116802.
- (61) Meevasana, W.; King, P.; He, R.; Mo, S.; Hashimoto, M.; Tamai, A.; Songsiririthigul, P.; Baumberger, F.; Shen, Z. Creation and Control of a Two-Dimensional Electron Liquid at the Bare  $\text{SrTiO}_3$  Surface. *Nat. Mater.* **2011**, *10*, 114–118.
- (62) King, P.; He, R. H.; Eknaphakul, T.; Buaphet, P.; Mo, S. K.; Kaneko, Y.; Harashima, S.; Hikita, Y.; Bahramy, M. S.; Bell, C.; et al. Subband Structure of a Two-Dimensional Electron Gas Formed at the Polar Surface of the Strong Spin-Orbit Perovskite  $\text{KTaO}_3$ . *Phys. Rev. Lett.* **2012**, *108*, 117602.
- (63) Wang, L.-Q.; Baer, D. R.; Engelhard, M. H.; Shultz, A. N. The Adsorption of Liquid and Vapor Water on  $\text{TiO}_2(110)$  Surfaces: The Role of Defects. *Surf. Sci.* **1995**, *344*, 237–250.
- (64) Ketteler, G.; Yamamoto, S.; Bluhm, H.; Andersson, K.; Starr, D. E.; Ogletree, D. F.; Ogasawara, H.; Nilsson, A.; Salmeron, M. The Nature of Water Nucleation Sites on  $\text{TiO}_2(110)$  Surfaces Revealed by Ambient Pressure X-ray Photoelectron Spectroscopy. *J. Phys. Chem. C* **2007**, *111*, 8278–8282.
- (65) Walle, L. E.; Borg, A.; Uvdal, P.; Sandell, A. Experimental Evidence for Mixed Dissociative and Molecular Adsorption of Water

on a Rutile  $\text{TiO}_2(110)$  Surface Without Oxygen Vacancies. *Phys. Rev. B* **2009**, *80*, 235436.

(66) Anisimov, V. I.; Zaanen, J.; Andersen, O. K. Band Theory and Mott Insulators: Hubbard U Instead of Stoner I. *Phys. Rev. B* **1991**, *44*, 943–954.

(67) Cuong, D.; Lee, B.; Choi, K.; Ahn, H.-S.; Han, S.; Lee, J. Oxygen Vacancy Clustering and Electron Localization in Oxygen-Deficient  $\text{SrTiO}_3$ : LDA+ U Study. *Phys. Rev. Lett.* **2007**, *98*, 115503.

(68) Kurtz, R. L.; Stock-Bauer, R.; Msdey, T. E.; Román, E.; De Segovia, J. L. Synchrotron Radiation Studies of  $\text{H}_2\text{O}$  Adsorption on  $\text{TiO}_2(110)$ . *Surf. Sci.* **1989**, *218*, 178–200.

(69) Di Valentin, C.; Pacchioni, G.; Selloni, A. Electronic Structure of Defect States in Hydroxylated and Reduced Rutile  $\text{TiO}_2(110)$  Surfaces. *Phys. Rev. Lett.* **2006**, *97*, 166803.

(70) Kowalski, P. M.; Camellone, M. F.; Nair, N. N.; Meyer, B.; Marx, D. Charge Localization Dynamics Induced by Oxygen Vacancies on the  $\text{TiO}_2(110)$  Surface. *Phys. Rev. Lett.* **2010**, *105*, 146405.

(71) Reuter, K.; Scheffler, M. Composition, Structure, and Stability of  $\text{RuO}_2(110)$  as a Function of Oxygen Pressure. *Phys. Rev. B* **2001**, *65*, 035406.

(72) Stull, D. R.; Prophet, H. *JANAF Thermochemical Tables*, 2<sup>th</sup> ed; U.S. National Bureau of Standards: Washington, DC, 1971.

(73) Merte, L. R.; Peng, G.; Bechstein, R.; Rieboldt, F.; Farberow, C. A.; Grabow, L. C.; Kudernatsch, W.; Wendt, S.; Lægsgaard, E.; Mavrikakis, M.; et al. Water-Mediated Proton Hopping on an Iron Oxide Surface. *Science* **2012**, *336*, 889–893.

(74) Wendt, S.; Matthiesen, J.; Schaub, R.; Vestergaard, E.; Lægsgaard, E.; Besenbacher, F.; Hammer, B. Formation and Splitting of Paired Hydroxyl Groups on Reduced  $\text{TiO}_2(110)$ . *Phys. Rev. Lett.* **2006**, *96*, 066107.

(75) Lu, G.; Linsebigler, A.; Yates, J. T., Jr.  $\text{Ti}^{3+}$  Defect Sites on  $\text{TiO}_2(110)$ : Production and Chemical Detection of Active Aites. *J. Phys. Chem.* **1994**, *98*, 11733–11738.

(76) Chambers, S. A.; Ohsawa, T.; Wang, C. M.; Lyubinetsky, I.; Jaffe, J. E. Band Offsets at the Epitaxial Anatase  $\text{TiO}_2/n\text{-SrTiO}_3(001)$  Interface. *Surf. Sci.* **2009**, *603*, 771–780.

(77) Abad, J.; Böhme, O.; Román, E. Dissociative Adsorption of NO on  $\text{TiO}_2(110)\text{-(1}\times\text{2)}$  Surface:  $\text{Ti}_2\text{O}_3$  Rows as Active Sites for the Adsorption. *Langmuir* **2007**, *23*, 7583–7586.